Drug Delivery and Translational Research (2024) 14:2558–2577
https://doi.org/10.1007/s13346-024-01529-6

ORIGINAL ARTICLE

A comparative study of passive drug diffusion through human skin via intercellular and sweat duct route: effect of aging

Aditya Ranjan[1] · Vijay S. Duryodhan[1] · Nagesh D. Patil[2]

Accepted: 21 January 2024 / Published online: 16 February 2024

Abstract

A method of drug delivery that could provide control over medicine reaching the bloodstream for systemic circulation would be of immense importance. This work presents a comparative study of the temporal and spatial variation of drugs diffusing passively through two separate routes of human skin, namely intercellular (ICR) and sweat duct route (SDR). An analysis is carried out for two age groups (young < 40 years and old > 60 years of age). Governing equations based on Fick's law for mass transfer have been solved numerically using an in-house developed code. The code has been validated thoroughly with numerical and experimental work from the literature. Each skin route is modeled into three compartments sandwiched between the donor and receiver compartments. To understand the role of diffusion and partition coefficient on drug permeation, four drugs, namely hydrocortisone, trans-cinnamic acid, caffeine, and benzoic acid, are considered. The drug diffusion rate is found greater through ICR as compared to SDR. Further, the amount of drugs diffusing through both routes increases with age. Desirable drug characteristic is inferred to be a lower value of partition coefficient and a higher value of diffusion coefficient. This study could lead to real-time assessment of drugs reaching the bloodstream and beyond.

Keywords Transdermal drug delivery · Passive diffusion · Intercellular route · Sweat duct route · Human skin · Aging

Nomenclature

C	Drug Concentration
t	Time
x	Spatial position
D	Diffusion coefficient
D^*	Effective diffusion coefficient
K	Partition coefficient
R	Powder drug radius
K_t	Drug dissolution constant
C_{do}	Initial amount of drug in donor compartment
M	Undissolved drug mass
M_o	Initial amount of undissolved drug
V_d	Volume of donor compartment
K_d	Powder dissolution constant
V_r	Volume of receiver compartment
C_d	Drug concentration in donor compartment
C_r	Drug concentration in receiver compartment
S	Permeation area
h_{sc}	Thickness of stratum corneum
h_{ve}	Thickness of viable epidermis
C_{sc}	Drug concentration in stratum corneum at a particular x and t
C_{ve}	Drug concentration in viable epidermis at a particular x and t
C_{de}	Drug concentration in dermis at a particular x and t
D_{sc}	Diffusion coefficient of drug in stratum corneum
D_{ve}	Diffusion coefficient of drug in viable epidermis
D_{de}	Diffusion coefficient of drug in dermis
C^+	Non-dimensional drug concentration
t^+	Non-dimensional time
dt^+	Non-dimensional time step
V^+	Non-dimensional volume
x^+	Non-dimensional spatial position
C_r^b	Drug concentration in receiver compartment before sampling
C_r^a	Drug concentration in receiver compartment after sampling
ΔV_r	Volume of drug leaving receiver compartment for systemic circulation
ε	Porosity

✉ Nagesh D. Patil
nageshpatil@iitbhilai.ac.in

[1] Department of Mechanical Engineering, Indian Institute of Technology Bhilai, Bhilai 491001, India

[2] Department of Mechanical Engineering and Department of Bioscience & Biomedical Engineering, Indian Institute of Technology Bhilai, Bhilai 491001, India

ζ Apparent tortuosity
h_{uc} Thickness of upper coil duct
h_{dd} Thickness of dermal duct
h_{sd} Thickness of secretory coil duct
C_{uc} Drug concentration in upper coil duct at a particular x and t
C_{dd} Drug concentration in dermal duct at a particular x and t
C_{sd} Drug concentration in secretory coil duct at a particular x and t
D_w Diffusion coefficient of drug in aqueous phase

Introduction

Drugs have been an integral part of mankind for ages, being used to diagnose illness. These drugs can be administered into the human body for systemic circulation via different methods such as oral, inhalation, injection, and transdermal. The drug delivered via the oral route undergoes first-pass metabolism [1] at various organ sites, such as the liver (which is the primary site for drug metabolism [2]). Injections, even though they are a faster mode of drug delivery, are uncomfortable as they are an invasive method. Inhalation is a simpler and less invasive route of drug administration. However, it may sometimes need an energy source and drugs may be hindered by the defense mechanism of the respiratory tract [3]. The transdermal mode is a non-invasive, safer, more facile, and sometimes controlled method to deliver a drug that additionally avoids first-pass metabolism. However, this method of drug delivery is more suitable for drugs having a low molecular weight (< 500 Da) and adequate lipophilicity and is effective at a low dosage. To deliver drugs of higher molecular weight or drugs which are hydrophilic or polar, the active modes of drug delivery such as iontophoresis, microneedling, thermal ablation, and cavitational ultrasound are used [1].

Even though topical solutions and ointments were being used to treat several illnesses from ancient times, but commercially the modern transdermal systems evolved in the 1970s. In terms of applications, transdermal patches are widely used to deliver drugs through the skin. In vitro flux of various drugs such as scopolamine, nitroglycerine, fentanyl, and estradiol was investigated in 1975. These drugs are now being delivered via transdermal systems as study showed that these compounds show significant permeation through the skin. This led to the introduction of a 3-D patch to deliver scopolamine to treat motion sickness. Transdermal patches became increasingly popular after the introduction of nicotine patches in the year 1989. As per current data, around 17 different drugs are being delivered through transdermal patches, with approximately 1 billion patches being manufactured each year [9]. Below we have presented the literature in two parts to set forth the objectives of the present work, one is to shed light on skin anatomy and second is methods to analyze transdermal drug delivery. These topics have been discussed in the below subsections.

Human skin is an anisotropic and heterogeneous material [4]; hence, it becomes very difficult to understand the permeation process occurring inside it. When a certain volume of topical solution is placed on the stratum corneum, it will try to diffuse through all the possible routes that it encounters, which adds an extra challenge to analyzing the role of the different routes in drug permeation. However, as the transcellular route offers large resistance [5], the intercellular route, sweat duct, and hair follicle route become more suitable pathways. For a 1-cm^2 surface area of skin for drug diffusion, the areas occupied by the hair follicles (0.05–1.5%) and sweat ducts (0.03–2%) are very small; hence, the major volume of the drug will diffuse through the intercellular route [6, 7]. Therefore, researchers often ignore the role of appendages in drug diffusion. Thus, the purpose of this numerical study is to understand the significance of appendages (in particular SDR) in drug permeation and to compare the drug diffusion through the intercellular route and appendage. We try to further enhance our understanding of the factors that influence passive diffusion and talk about the scope of delivering a drug through the appendage.

Stratum corneum mainly consists of dead keratinocyte cells that are separated from one another by a thin layer of intercellular lipids. This is sometimes referred to as the "Brick–Mortar" model [8] of the stratum corneum, as shown in Fig. 1. As the stratum corneum offers the main barrier to drug permeation, various methods mainly focus on overcoming this barrier [1, 9]. The rest of the layers in the epidermis (apart from the stratum corneum) are referred to as the "viable epidermis," whose thickness ranges between 50 and 100 µm. Resistance offered by both stratum corneum and viable epidermis to permeation of small and macromolecules has been investigated previously [10]. Beneath the epidermis layer lies the dermis, whose thickness ranges from 1 to 2 mm.

Appendages at the top of human skin emerge from the epidermis and dermis and mainly comprise eccrine and apocrine glands, ducts, and pilosebaceous units [11]. The main function of the eccrine sweat glands or ducts is to regulate the heat [12]. These tubular or ductal structures (as depicted in Fig. 1) consist of three composite parts, namely the upper coil duct, dermal duct, and secretory coil duct [13]. Previous studies on the morphology of the eccrine sweat gland provide insights into the various barrier elements along the sweat duct pathway. Barrier elements like tight junction proteins are present in sweat glands as well, which restrict the permeation of a compound [14]. These works suggest that sweat ducts can be an alternate penetration pathway. For a compound permeating through hair follicles, the main

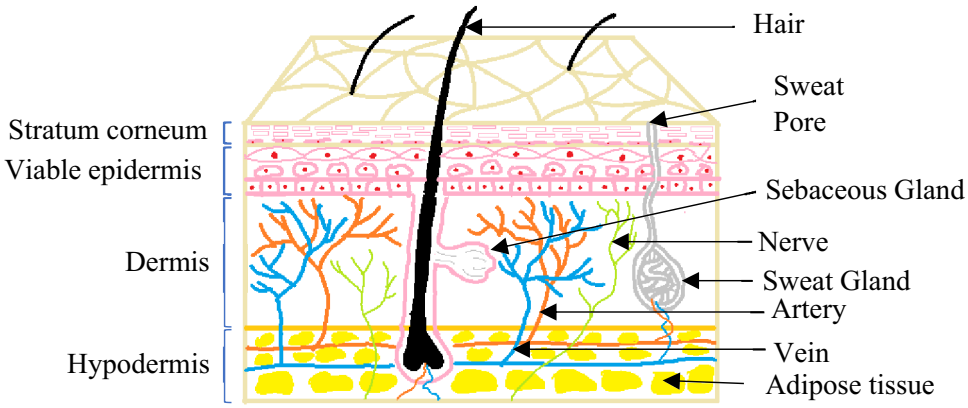

Fig. 1 Anatomy of human skin

barriers are the drug particle size [15], sebum [16], and hair cycle [11].

Due to various risks related to drug interaction with human skin as well as due to ethical issues, in vivo studies of drug diffusion through human skin are non-trivial. Therefore, there is a need for various alternatives methods to understand the drug permeation process through skin. Various methodologies, such as analytical [17], numerical [18], and experimental using artificial skin [19], are adopted in the literature to understand this phenomenon. Moreover, some animal skins, like rat skin or porcine skin, are found to closely resemble the characteristics of human skin [20]. Hence, it provides a good alternative to experimentally carrying out such studies. In vitro study involves the use of apparatus like the Franz cell diffusion apparatus, which consists of a cell membrane (human or animal skin sample through which drug permeation is to be studied) separated by donor and receiver compartments [21]. Further, analytical and numerical methods have also been used to study this complex phenomenon, and studies suggest that the results of experimental and numerical methods are in good agreement.

Some studies based on mathematical models [17, 18, 22–24] have been done which provide insights of passive drug diffusion through skin or membrane. For instance, both numerical and analytical approaches have previously been documented to study the passive diffusion of drugs through a swollen membrane sandwiched between two stagnant layers (a trilaminate system) [23]. Later, a similar diffusive mathematical model was used to determine the Acyclovir permeation properties through the rat skin [18]. A thermostatic Franz cell apparatus was used to perform the permeation experiments. They validated the results from the mathematical model with that of in vitro experiments which were found to be in good agreement.

Based on the above discussion, we can conclude that a drug diffusion through skin encounters mainly four routes (as depicted in Fig. 2), namely the intercellular route (ICR), transcellular route, and appendage route, which includes the hair follicle route (pilosebaceous unit) and sweat duct route (SDR) [25]. From the literature survey, it was found that majority of the previous studies were focused on analyzing diffusion through the overall skin and hair follicle route. Comprehensive reporting of passive drug diffusion through the sweat duct route is not found, as is the effect of aging on drug diffusion through the ICR and the SDR. A diffusion-based model is required for studying transdermal drug delivery (without considering the advection effects) because the skin is a region of very low permeability and hence advection effects can be neglected and a purely diffusion-based mathematical model can be implicated [26]. In the present study, the passive drug diffusion through the ICR and SDR has been studied using a mathematical diffusion model based on Fick's law [18]. The main objective of the work is to know which route among the two provides a faster drug delivery. This work also investigates the effect of aging on drug diffusion for which two age groups have

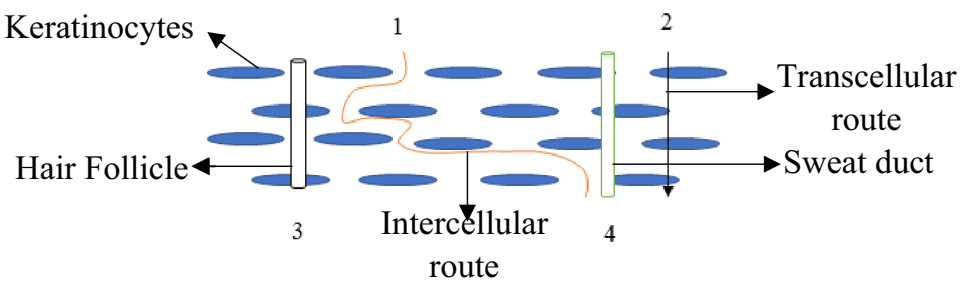

Fig. 2 Various routes of transdermal drug delivery

been considered, i.e., young age (< 40 years) and old age (> 60 years). The diffusion of four different drugs, namely hydrocortisone (HC), benzoic acid (BA), caffeine (CA), and trans-cinnamic acid (TCA), has been studied to understand the role of partition and diffusion coefficient on the amount of drug permeating through different layers of skin.

Physical and computational description of the problem

In the present numerical analysis, it has been assumed that the drug will passively diffuse through either the ICR or SDR. Figure 3 shows the schematic diagram of the ICR and SDR used in our numerical model. The variation of drug concentration as a function of space and time across these two routes can be described mathematically [18]. We use a one-dimensional second-order partial differential equation (PDE) based on Fick's law to determine the drug concentration both spatially and temporally simultaneously. The skin is assumed to be isotropic and homogeneous in nature to reduce the complexity of the mathematical model [18]. For drug diffusion via the ICR, the human skin is divided into three layers: stratum corneum (sc), the viable epidermis (ve), and dermis (de), each with its own partition and diffusion coefficient (Fig. 3a). Here, each of the layers corresponds to a compartment. So, a particular pathway is assumed to have a total of five compartments, with donor and receiver compartments being at the top and bottom, respectively, of the three compartments classified above. The SDR has also been divided into three layers: upper coil duct (uc), dermal duct (dd), and secretory coil duct (sd) (Fig. 3b) [13]. While studying drug diffusion through the SDR, the drug's diffusion coefficient in water has been considered. This is because almost 99% of the medium of the sweat duct is aqueous. Also, the effect of porosity and tortuosity has been considered to increase the robustness of the model. However, due to the lack of data in literature, the partition and diffusion coefficients of drugs permeating through the skin layers for young as well as old age people have been assumed to be the same for both routes. In the present numerical study, certain conditions similar to in vitro experiments [18] (such as drug dissolution in donor compartment and receiver sampling technique) have been considered. Throughout the analysis, the effect of drug dissolution is considered in the donor compartment, as some amount of undissolved drug mass is always present in the donor compartment. The receiver sampling technique [18] has also been adopted in our numerical model to account for the replacement of a certain amount of drug entering the blood capillaries with a fresh amount of solvent (as shown in Fig. 3). In this study, we conducted a detailed investigation into drug permeation through the ICR and SDR routes using a numerical approach. The study involved the development and utilization of an in-house MATLAB code to solve the diffusion equations governing drug transport through the skin layers. Specifically, the code considered the complexities of the ICR and SDR, accounting for different layers and their associated barriers (such as partition coefficients in the case of ICR) and geometrical parameters (such as porosity and tortuosity of SDR).

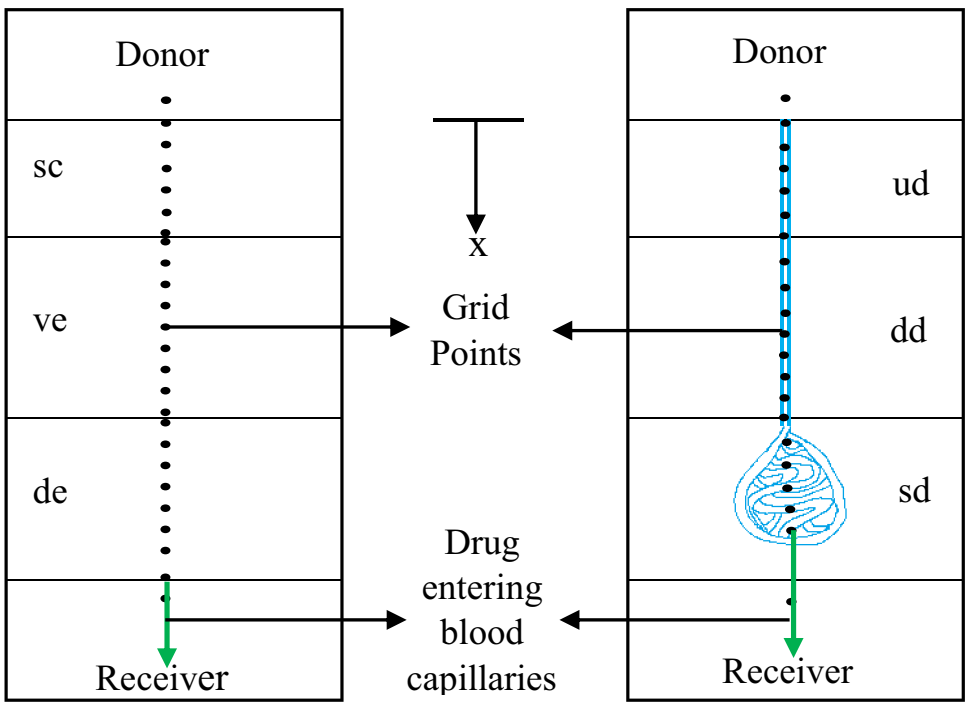

Fig. 3 Schematic representation of compartment model: **a** Intercellular route. **b** Sweat duct route

One of the major limitations of transdermal drug delivery is that all drugs do not easily diffuse through the skin. It is found that the drugs having a low molecular weight (< 500 Da), appropriate solubility in both oil and water, and balanced lipophilicity are found to be suitable for delivery through skin [27]. We have tried to analyze the permeation of four different drugs through both the ICR and SDR. Table 1 illustrates the molecular weight and applications of drugs considered in the present analysis. It is to be noted that all the drugs mentioned in Table 1 show adequate lipophilicity and have a molecular weight of less than 500 Da. Hence, they can be adopted for practical dermatological applications in the future as well.

Experimental documentation exists for the partition and diffusion coefficients of 50 chemicals in intact skin and isolated skin layers [28]. In the present study, out of the 50 chemicals, four have been selected and their respective data for partition coefficient (K) and diffusion coefficient (D) in stratum corneum, viable epidermis, and dermis (depicted by subscript 1, 2, and 3 respectively) have been mentioned in Table 1. This table also enlists the diffusion coefficient of these drugs in an aqueous phase [29–31], which is the permeating medium of a drug through the sweat duct (research suggest that sweat duct can be considered as a tube filled with water [32]). These four drugs are more commonly used in treatment of applications as mentioned in Table 1.

The drugs mentioned above are initially assumed to be in powder form. Our work focusses on numerically analyzing the permeation of drug solutions prepared by dissolving the drugs listed in Table 1. A solution of the above drugs can be prepared by dissolving the drug in a media containing DPBS and sodium azide [28]. This work proceeds with modelling the permeation of a drug with an initial size (R_o) of 5.7 μm and a powder dissolution constant (K_d) of 5.01×10^{-5} cm/s (which is assumed to be constant for all the drugs) [18]. Arbitrarily, the initial drug concentration in the donor compartment (C_{do}) is taken to be 2.62 mg/cm^3. The volume of the donor (V_d) and receiver (V_r) compartments is assumed to be 3 cm^3 (subscripts d and r correspond to the donor and receiver compartments respectively). While the experimental setup, such as in the Franz cells apparatus, often features a larger receiver compartment, it is not realistic to assume a larger volume for the receiver compartment to mimic that of human skin. Therefore, in our simplified model, we have assumed equal volumes (V_d and V_r). It has also been assumed that initially, 1 mg of the undissolved drug (M_o) is present in the donor compartment, while the drug permeation area (S) is taken as 1 cm^2.

Numerical details

This section discusses the numerical model and methodology adopted to generate the solution for the set of PDEs describing the permeation through ICR and SDR. It also includes the validation of the in-house developed Matlab code used to obtain the numerical solutions by comparing the present results with the published numerical and experimental findings. Additionally, we have also performed the grid and time independence test which has been discussed at the end of this section. An in-house MATLAB code is developed to determine the final amount of drug solution reaching the receiver compartment for systemic circulation via blood stream. The code aims at solving a set of discretized non-dimensional equations (Eqs. 18–31 for ICR and Eqs. 35–50 for SDR) to obtain the drug concentration variation in different layers of compartment model (Fig. 3) describing the ICR and SDR in our proposed numerical model.

Table 1 Partition coefficient and diffusion coefficient of drugs in skin layers. Aqueous diffusion coefficient of drugs

Drugs	Molecular weight (in Da)	Partition coefficient	Diffusion coefficient (cm^2/s)	Diffusion coefficient in water (cm^2/s)	Applications
Hydrocortisone	362.46	$K_1 = 8.22$ $K_2 = 3.94$ $K_3 = 3.11$	$D_1 = 4.12 \times 10^{-5}$ $D_2 = 9.61 \times 10^{-6}$ $D_3 = 8.45 \times 10^{-3}$	$D_w = 4.6 \times 10^{-6}$	Treat polyarthritis on the fingers [33]
Benzoic acid	122.12	$K_1 = 5.04$ $K_2 = 0.96$ $K_3 = 1.52$	$D_1 = 4.48 \times 10^{-4}$ $D_2 = 9.63 \times 10^{-4}$ $D_3 = 4.85 \times 10^{-2}$	$D_w = 1.16 \times 10^{-5}$	A test substance, often used in skin penetrant studies [34]
Caffeine	194.19	$K_1 = 7.84$ $K_2 = 0.94$ $K_3 = 1.12$	$D_1 = 9.83 \times 10^{-5}$ $D_2 = 4.23 \times 10^{-5}$ $D_3 = 7.96 \times 10^{-3}$	$D_w = 9 \times 10^{-6}$	Prevents excessive fat accumulation in skin, promotes lymphatic drainage, and protects skin from photodamage [35]
Trans-cinnamic acid	148.16	$K_1 = 7.26$ $K_2 = 2.83$ $K_3 = 3.47$	$D_1 = 9.81 \times 10^{-5}$ $D_2 = 5.4 \times 10^{-5}$ $D_3 = 9.82 \times 10^{-3}$	$D_w = 9.9 \times 10^{-6}$	Fragrance agents [36]

Governing equations

Our study utilizes a one-dimensional compartment model to geometrically classify considered skin routes into three different compartments. The drug concentration variations across the ICR and SDR are modeled by Eqs. 1 and 2 respectively. Here, C represents the drug concentration at a particular location and at a particular time. X, t, and D represent the spatial position, time, and drug diffusion coefficient respectively. To account for the porosity and tortuosity associated with the sweat duct, the effective diffusion coefficient (D^*) term is introduced for the SDR (as shown in Eq. 2) which will be discussed in detail in the "Sweat duct route" section.

$$\frac{\partial C}{\partial t} = D\frac{\partial^2 C}{\partial x^2} \tag{1}$$

$$\frac{\partial C}{\partial t} = D^*\frac{\partial^2 C}{\partial x^2} \tag{2}$$

In the donor compartment (topmost compartment), the solution of the test drug is assumed to be present. Our numerical investigation prioritizes the estimation of the dissolution process, crucial for determining drug concentration in the donor compartment. Factors such as particle size distribution, shape, and aggregation influence this complex mechanism. Key to this process is the reduction in solid particle radius during dissolution, governed by the parameter K_t. The rate of dissolution of the initially powdered test drug in the solvent is hence described by the drug dissolution constant K_t (as shown in Eq. 3). The drug particle radius (R) is a function of the ratio of mass of drug to initial amount of undissolved drug and is given by Eq. 4 [18].

$$K_t = 4\pi R^2\frac{K_d}{V_d} \tag{3}$$

$$R = R_0\sqrt[3]{\frac{M}{M_0}} \tag{4}$$

It is assumed that some amount of undissolved drug is present in the donor compartment. Consequently, the drug mass has to be balanced using the mass balance equation

$$M = M_0 + V_d\left(C_{do} - C_d\right) - V_r C_r - \int_0^{h_{sc}} C_{sc}S\,dx - \int_{h_{sc}}^{h_{sc}+h_{ve}} C_{ve}S\,dx - \int_{h_{sc}+h_{ve}}^{h_{sc}+h_{ve}+h_{de}} C_{de}S\,dx \tag{5}$$

where M represents the net amount of undissolved drug in the donor compartment. Equation 5 also takes into account the mass of drug present in the donor and receiver compartments, while integrals take into account the mass diffusing through each of the layers of skin. V_d and V_r represent the volume of the donor and receiver compartments, respectively. C_{do} and C_d represent the initial and instantaneous concentration of solution of test drug present in the donor compartment. While, as per Fick's diffusion equation, to take into account the spatial variation of drug concentration, integral is done over different skin layers' thicknesses.

Equation 6 describes the temporal variation of drug concentration in the donor compartment (C_d). C_s represents the drug solubility, which is assumed to be the same as the initial drug concentration (C_{do}), while D_{sc} and C_{sc} represent the drug diffusion coefficient and concentration, respectively, in the stratum corneum layer. Upon reaching the interface of donor and stratum corneum (in the case of the ICR), the drug will be subjected to a permeability barrier by the stratum corneum. Here, it is accounted by the partition coefficient (K) and is given by Eq. 7. The partition coefficient is defined as the ratio of the solute concentration on either side of an interface at the equilibrium condition. However, as drug partitioning varies with varying interface, the different partition coefficients are considered, as shown in Eq. 7.

$$V_d\frac{dC_d}{dt} = V_d K_t\left(C_s - C_d\right) + D_{sc}S\frac{\partial C_{sc}}{\partial x}\Big|_{x=0} \tag{6}$$

$$k_1 = \frac{C_d}{C_{sc}};\ k_2 = \frac{C_{sc}}{C_{ve}};\ k_3 = \frac{C_{ve}}{C_{de}};\ k_r = \frac{C_{de}}{C_r} = 1 \tag{7}$$

The variation of the drug concentration in the stratum corneum (sc), the viable epidermis (ve), and dermis (de) is given by Eqs. 8, 10, and 12. The continuity of drug concentration between different layers is ensured by interface conditions such as Eq. 9 between stratum corneum and viable epidermis, and Eq. 11 between viable epidermis and dermis.

$$\frac{\partial C_{sc}}{\partial t} = \frac{\partial}{\partial x}\left(D_{sc}\frac{\partial C_{sc}}{\partial x}\right) \tag{8}$$

$$D_{sc}\frac{\partial C_{sc}}{\partial x}\Big|_{x=h_{sc}} = D_{ve}\frac{\partial C_{ve}}{\partial x}\Big|_{x=h_{sc}} \tag{9}$$

$$\frac{\partial C_{ve}}{\partial t} = \frac{\partial}{\partial x}\left(D_{ve}\frac{\partial C_{ve}}{\partial x}\right) \tag{10}$$

$$D_{ve}\frac{\partial C_{ve}}{\partial x}\Big|_{x=h_{sc}+h_{ve}} = D_{de}\frac{\partial C_{de}}{\partial x}\Big|_{x=h_{sc}+h_{ve}} \tag{11}$$

$$\frac{\partial C_{de}}{\partial t} = \frac{\partial}{\partial x}\left(D_{de}\frac{\partial C_{de}}{\partial x}\right) \tag{12}$$

The variation of drug concentration in the receiver compartment (C_r) is given in Eq. 13. C_r represents the amount of drug just entering the receiver compartment and becoming available for systemic circulation. Here, it has been assumed that initially, the C_{do} amount of drug is present only in the donor compartment and there is no trace of the test drug in the rest of the layers, as shown in Eq. 14.

$$V_r \frac{\partial C_r}{\partial t} = D_{de} S \frac{\partial C_{de}}{\partial x}\Big|_{x=h_{sc}+h_{ve}+h_{de}} \tag{13}$$

$$C_d = C_{d0};\ C_{sc} = C_{ve} = C_{de} = C_r = 0 \tag{14}$$

The similar set of PDEs (Eqs. 1–14) have been used to describe the diffusion through the SDR as well. Due to its tubular nature, there is no such interface present inside the sweat duct. Hence, there is no role for the partition coefficient in the case of the sweat duct. However, to consider the sudden changes in porosity and tortuosity of various layers, the continuity of drug concentration is ensured by interface conditions here as well (similar to Eqs. 9 and 11). The above set of partial differential equations (PDEs) are made non-dimensional using a set of characteristic variables shown in Eqs. 15 and 16 and then discretized using the central difference and backward difference schemes. These discretized equations are solved using the finite difference method (FDM) in explicit form using an in-house developed Matlab code to obtain the solutions.

$$C_d^+ = \frac{C_d}{C_{do}};\ C_r^+ = \frac{C_r}{C_{do}};\ t^+ = t\frac{D_{ve}}{h_{ve}^2} \tag{15}$$

$$V_d^+ = \frac{V_d}{sh_{ve}};V_r^+ = \frac{V_r}{sh_{ve}};x^+ = 1 + \frac{x}{h_{ve}};\ K_t^+ = K_t\frac{h_{ve}^2}{D_{ve}} \tag{16}$$

Some amount of drug will be leaving the receiver compartment and entering the blood capillaries surrounding the coiled duct in the case of the SDR [37] (or the dermis in the case of the ICR) as well as other targeted regions. To account for the aforementioned phenomena, a receiver sampling technique is employed, in which a fixed amount of drug (around 10%) entering the receiver compartment is assumed to be transferred to the targeted area after each time step, as shown in Eq. 17 [18].

$$C_r^a = \frac{C_r^b\left(V_r - \Delta V_r\right)}{V_r} \tag{17}$$

where $C_r{}^b$ and $C_r{}^a$ represent the drug concentration in the receiver compartment before and after sampling, while ΔV_r represents the volume being carried away for circulation.

Intercellular route

The most preferable route for transdermal drug diffusion is the ICR. In this route, the drug passes through the region around corneocytes (a lipid-rich region) present in the stratum corneum [21]. The drug permeating through the ICR will encounter three-phase regions of protein, lipid, and water. To numerically model the drug diffusion through the ICR, the one-dimensional second law of Fick's diffusion is used, which is given by Eq. 1. The schematic shown in Fig. 3a represents the compartment model used to study drug diffusion for ICRs.

The produced non-dimensional discretized set of PDEs for the ICR has been presented by Eqs. 18–31.

Donor compartment

$$K_t^+ = \frac{4\Pi R_0^2 K_d h_{ve}^2}{D_{ve} V_d} \cdot R^{+2} \tag{18}$$

$$R^+ = \sqrt[3]{M^+} \tag{19}$$

$$M^+ = 1 + \left(\frac{C_{d0} Sh_2}{M_0}\left(V_d^+\left(1 - C_d^+\right) - V_r^+ C_r^+ - \int_0^{h_{sc}} C_{sc}^+ dx^+ - \int_{h_{sc}}^{h_{sc}+h_{ve}} C_{ve}^+ dx^+ - \int_{h_{sc}+h_{ve}}^{h_{sc}+h_{ve}+h_{de}} C_{de}^+ dx^+\right)\right. \tag{20}$$

$$C_d^{+n+1} = C_d^{+n} + k_t^+ \Delta t^+\left(C_s^+ - C_d^+\right) + \frac{D_{sc}\Delta t^+}{D_{ve} V_d^+} \cdot \frac{\left(C_{sc,i+1} - C_{sc.i}\right)}{\Delta x_{sc}^+} \tag{21}$$

Boundary of donor compartment and layer 1

$$C_d^+|_{x^+=1} = k_1 C_1^+ \tag{22}$$

Layer 1 (stratum corneum)

$$C_{sc,i}^{+n+1} = C_{sc,i}^{+n} + \frac{D_{sc}\Delta t^+}{D_{ve}\Delta x_1^{+2}} \cdot \left(C_{sc,i-1}^{+n} - 2C_{sc,i}^{+n} + C_{sc,i+1}^{+n}\right) \tag{23}$$

Boundary of layer 1 and layer 2

$$C_{sc}^+|_{x^+=h_{sc}^+} = k_2 C_{ve}^+|_{x^+=h_{sc}^+} \tag{24}$$

$$C_{sc,i}^{+n} = (C_{sc,i+2}^{+n} + \frac{D_{sc}\Delta x_{ve}^+}{D_{ve}\Delta x_{sc}^+} \cdot C_{sc,i-1}^{+n})/(k_2 + \frac{D_{sc}\Delta x_{ve}^+}{D_{ve}\Delta x_{sc}^+}) \tag{25}$$

Layer 2 (viable epidermis)

$$C_{ve,i}^{+n+1} = C_{ve,i}^{+n} + \frac{D_{ve}\Delta t^+}{D_{ve}\Delta x_{ve}^{+2}} \cdot \left(C_{ve,i-1}^{+n} - 2C_{ve,i}^{+n} + C_{ve,i+1}^{+n}\right) \tag{26}$$

Boundary of layer 2 and layer 3

$$C^{+}_{ve}|_{x^{+}=h^{+}_{ve}} = k_3 C^{+}_{de}|_{x^{+}=h^{+}_{ve}} \tag{27}$$

$$C^{+n}_{ve,i} = (C^{+n}_{ve,i-1} + \frac{D_{de}\Delta x^{+}_{ve}}{D_{ve}\Delta x^{+}_{de}} \cdot C^{+n}_{de,i+2})/(1 + k_3 * \frac{D_{de}\Delta x^{+}_{ve}}{D_{ve}\Delta x^{+}_{de}}) \tag{28}$$

Layer 3 (dermis)

$$C^{+n+1}_{de,i} = C^{+n}_{de,i} + \frac{D_{de}\Delta t^{+}}{D_{ve}\Delta x^{+2}_{de}} \cdot \left(C^{+n}_{de,i-1} - 2C^{+n}_{de,i} + C^{+n}_{de,i+1}\right) \tag{29}$$

Boundary of layer 3 and receiver compartment

$$C^{+n}_{r,i} = C^{+n}_{de,i-1} \tag{30}$$

Receiver compartment

$$C^{+n+1}_{r,i} = C^{+n}_{r,i} + \frac{D_{de}\Delta t^{+}}{V^{+}_{r}D_{ve}} \cdot \frac{\left(C^{+n}_{de,i-2} - C^{+n}_{de,i-1}\right)}{\Delta x^{+}_{de}} \tag{31}$$

Sweat duct route

Eccrine sweat glands are present all over the body except areas such as lips or genital area and opens onto the top surface of human skin [38]. Some researchers have analyzed the anatomy of sweat duct and came to conclusion about it being a suitable pathway for drug permeation [14]. Hence, due to its abundance, it becomes interesting to check its efficacy as a suitable pathway for passive diffusion of drugs.

The drug diffusion pathway inside the sweat duct is tortuous which is longer than the non-tortuous path and it reduces the concentration gradient (considering the dynamics on molecular scales to be unchanged). Hence, the diffusion coefficient (D) will get reduced due to a tortuous network [26]. Also, due to presence of porosity, fluid passing through the porous media will be subjected to more drag; hence, diffusion will get reduced [39]. Hence, both porosity and tortuosity reduce the diffusion. The combined effect of porosity and tortuosity leads to decrease in amount of drug diffusing through the SDR.

In the present study, the effect of sorption (i.e., interaction of solute drug molecules with the walls) has not been considered. Hence, the retardation factor in the mathematical model used for sweat ducts is unity [40]. Hence, the modified diffusion equation obtained for describing passive drug diffusion through the sweat duct is given by Eq. 32.

$$\frac{\partial C}{\partial t} = \frac{D_e}{\varepsilon}\frac{\partial^2 C}{\partial x^2} \tag{32}$$

where D_e is defined as the product of aqueous diffusion coefficient of drugs (D_w, mentioned in Table 1), porosity (ε), and the apparent tortuosity (which is the inverse of tortuosity). Porosity of the sweat duct has been defined as the ratio of total area of sweat gland per square centimeter. Tortuosity has been defined as the ratio of tortuous path length (L_e) to the straight path length (L) [26]. "C" represents the drug concentration in a particular compartment at a particular instant of time. The effect of tight junction has been neglected in the case of SDR as there has not been such mathematical model yet developed to quantify for the resistance that it would impose against permeation of substances. Also, as mentioned in the previous section, partition coefficient has no role to play in the case of sweat duct. So, partition coefficient has been treated as unity in this case, i.e., $K_1 = K_2 = K_3 = 1$. A schematic shown in Fig. 3b highlights the compartment model used to study the drug diffusion through the SDR.

The obtained non-dimensional discretized set of PDEs for the SDR has been mentioned in the "Appendix" section (refer to Eqs. 35–50).

Effect of aging

The present work also discusses the effect of aging on drug diffusion. Hence, it becomes crucial to identify the parameters that vary with aging in the case of ICR and SDR and may result in an expected variation in drug concentration. According to Fick's law (Eq. 1), drug concentration depends upon diffusion coefficient of drug, thickness of the layer through which the drug is diffusing, and time. In the case of ICR, it is found that the thickness of each of the human skin layers, i.e., stratum corneum, viable epidermis, and dermis changes upon aging (as shown in Table 2). Hence, upon change of layer thickness, both spatial and temporal rate of drug permeation will also be affected.

As per Eq. 2, the spatial and temporal variation of drug diffusing through the sweat duct is found to depend upon the aqueous diffusion coefficient of the drug, the porosity, and tortuosity of the duct layer, as well as the thickness of each layer of the sweat duct and time. The geometrical parameters associated with the sweat duct are the duct length and diameter. Due to the change in thickness of various skin layers (as mentioned in Table 2), the tortuosity of various sections of the sweat duct also changes. Past research shows that the tortuous pathway changes upon aging [42]. Further, it has been reported that the pore size increases upon aging [43]. It is to be noted that to calculate the porosity of the sweat duct,

Table 2 Variation in thickness of skin layers upon aging

Compartment	Young age (< 40)	Old age (> 60)
Stratum corneum [41]	15 µm	17 µm
Viable epidermis [41]	62 µm	52 µm
Dermis [42]	982 µm	616 µm

Table 3 Variation in pore size and tortuosity upon aging

Compartment	Pore diameter (μm) [13]		Tortuosity [42]	
	Young	Old	Young	Old
Upper coil duct	20	60	1.22	1.39
Dermal duct	10	20	2.00	2.73
Secretory coil duct	30	40	5.06	3.82

its inner diameter has been considered. The inner diameter corresponds to the lumen of the sweat duct where sodium and chloride ions meet to form NaCl and an osmotic gradient is created that drives water inside the lumen [12]. So, the drug will also try to diffuse through the lumen region. A tight junction exists beyond this region, which will try to limit the permeation.

An upward shifting of the eccrine sweat gland (towards the skin's surface) is observed upon aging due to a decrease in the size of the dermis. The path lengths are calculated using image analysis (using ImageJ software) and the obtained tortuosity of each layer is mentioned in Table 3. It is to be noted that there is no significant difference in the number of sweat glands when compared between young (< 40 years) and old age (> 60 years) [42]. The number of sweat glands has been taken as 150 [13].

Solution steps

The process involved in the numerical methodology to obtain the solution is presented as a step-by-step approach in Fig. 4. It shows the systematic way for obtaining the solution.

It involves the selection of the route for drug diffusion, then, defining input variables governed by age and drugs such as partition and diffusion coefficient of drugs (Table 1), thickness of different layers of the skin (Table 2) and pore diameter, and tortuosity (Table 3). After this, a solution will be obtained by solving the set of discretized equations, i.e., Eqs. 18–31 (for ICR) and Eqs. 35–50 (for SDR) using a MATLAB-based (version R2021a) computer program developed in-house.

Validation

For checking its validity, the developed code is used to obtain results for drug diffusion through the swollen membrane [23] and rat skin [18] subjected to the same conditions as mentioned in the respective literature. The results obtained using the MATLAB code are then compared with the published results to establish the accuracy of the code. Grid independence and time independence tests are also done, which indicate that the developed code provides appropriate results for optimal mesh size and time step.

Validation with results of permeation study through swollen membrane

Previously, the drug permeation through a swollen membrane (trilaminate system) using linear and numerical models has been analyzed [23]. In their proposed numerical model, two cases were considered. In one of the cases, it was assumed that drug dissolution (K_t) in the donor compartment was non-zero (Fig. 5a), while in another case it was assumed to be zero (Fig. 5b). Figure 5 shows good agreement between the present work and numerical results for drug diffusion through a swollen membrane.

Validation with results of permeation study through a rat skin

An experimental analysis of acyclovir permeation on different rat skin samples using a thermostatic Franz cell apparatus was performed and has been documented. A purely diffusive mathematical model based on Fick's law was used to evaluate the diffusion through rat skin.

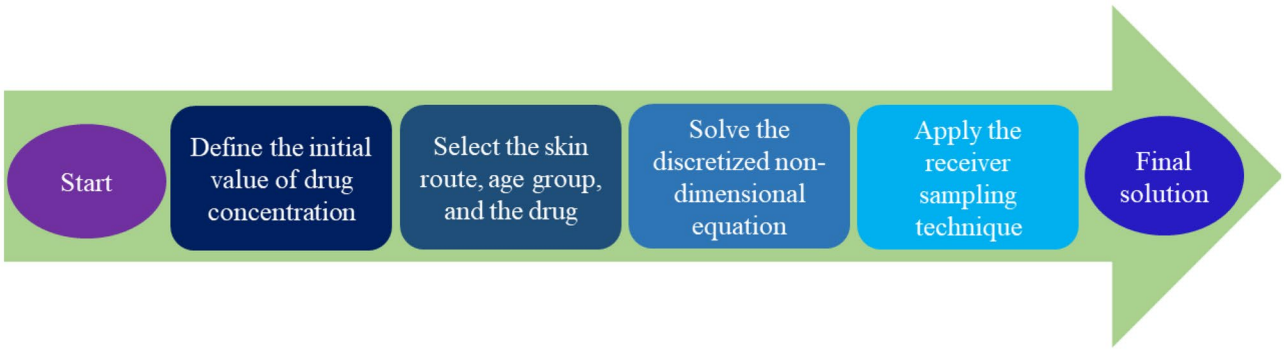

Fig. 4 Flow chart

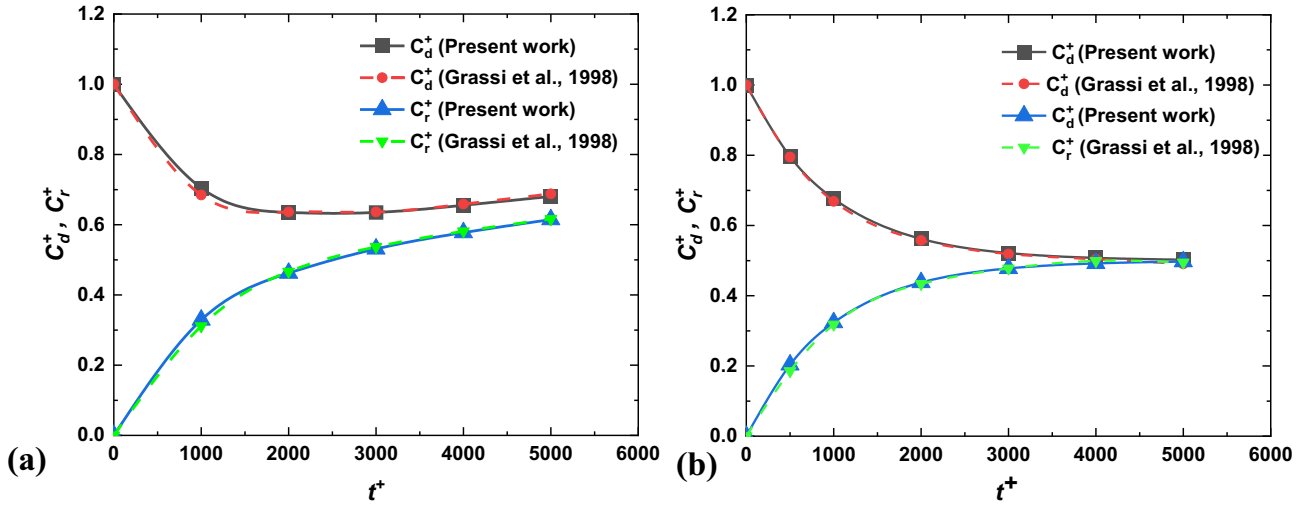

Fig. 5 Temporal variation of drug in donor and receiver compartment for **a** $K_t = 1.88 \times 10^{-4}$ and **b** $K_t = 0$

In-house Matlab code is used to obtain results for skin sample no. 9 mentioned in the literature [18]. Figure 6 shows a good agreement between the published experimental results and the present results obtained using Matlab code.

Grid and time independence study

An in-house Matlab code is validated for the time-independent and grid-independent tests. This validation is done for one of the drugs, which is hydrocortisone. Figures 7 and 8 depict the grid independence and time independence tests respectively done for results obtained after the numerical analysis of hydrocortisone diffusing through intercellular and sweat duct routes corresponding to geometrical parameters of a young age. The grid points in each layer are adjusted from $N = 6$ to 31 for the intercellular pathway.

Figure 7 depicts four temporal fluctuations in hydrocortisone concentration in the receiver compartment at various grid counts used to discretize the skin layers. It demonstrates that the results are unaffected by the number of grid points

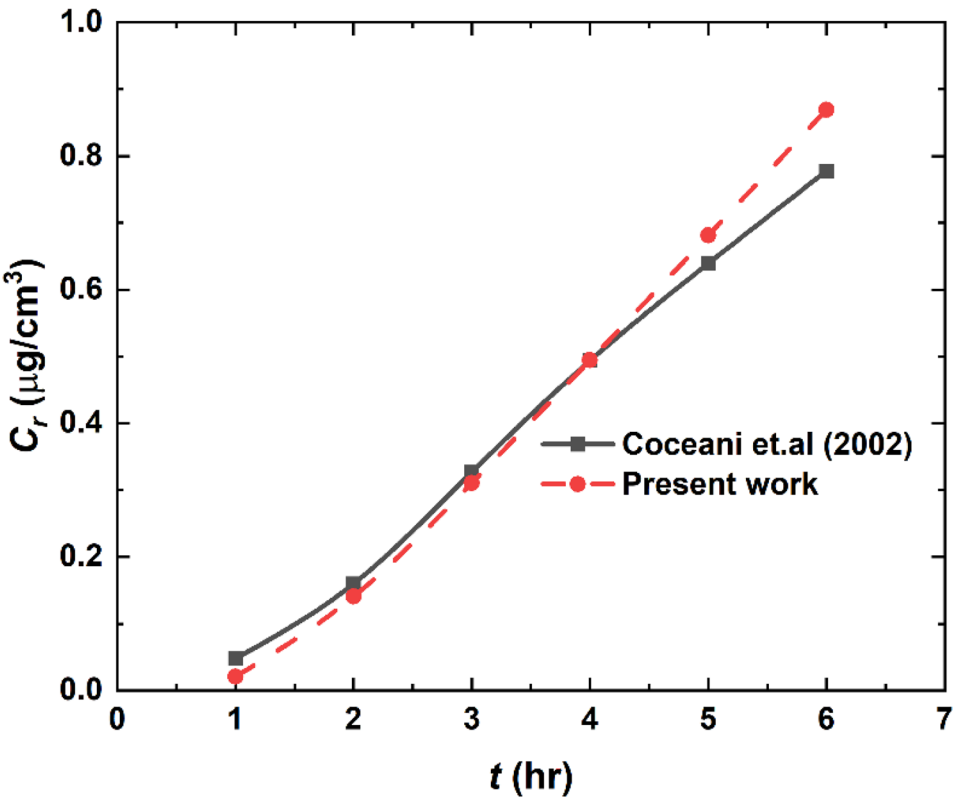

Fig. 6 Validation with results of acyclovir permeation through rat skin [18]

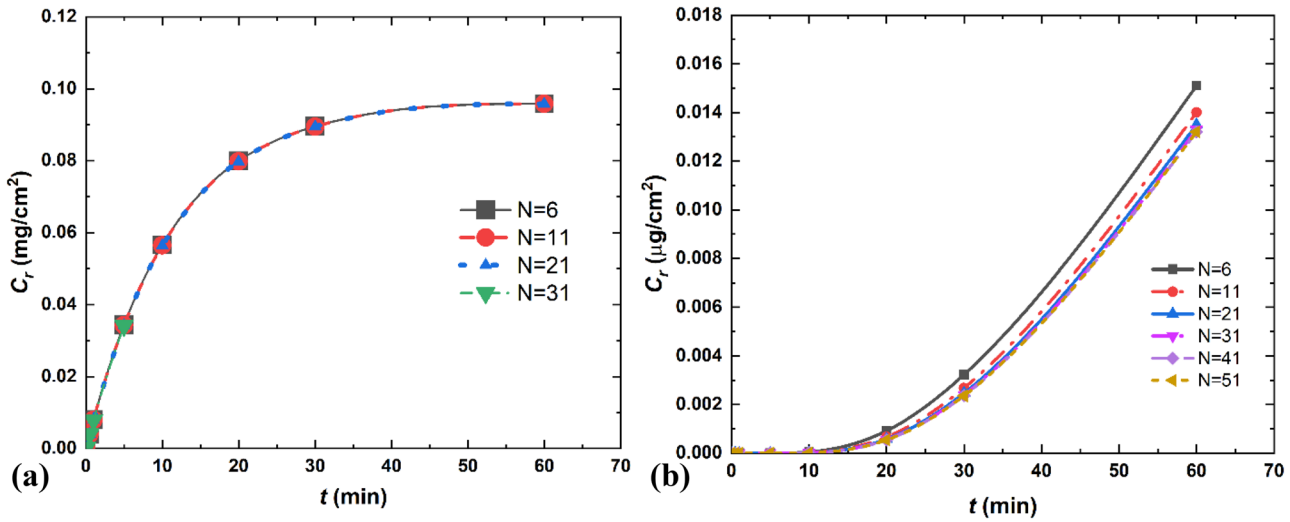

Fig. 7 Grid independence test for hydrocortisone diffusing through **a** intercellular route and **b** sweat duct route

for the ICR (as illustrated in Fig. 7a). Grid independence is achieved for sweat duct (Fig. 7b) beyond $N=21$.

The non-dimensional time step dt^+ is varied for ICR in the same way that grid independence is varied, and the time independence test curve is displayed in Fig. 8. Time independence behavior for ICR (Fig. 8a) can be noticed starting at $dt^+=10^{-5}$ while for SDR (Fig. 8b) at $dt^+=10^{-9}$.

Hence, based on the above test, the number of grid points chosen in each layer for ICR and SDR is 6 and 21. While the non-dimensional time steps for ICR and SDR are taken as 10^{-5} and 10^{-9}, respectively.

Results and discussion

The passive permeation of four drugs has been examined numerically and discussed in detail in this section for both young and old age human skin. At the end of this section, an overall comparison of the drug concentration distribution with time for all the four drugs is plotted and discussed to understand the effect of partition and diffusion coefficient on it.

Temporal and spatial variation of hydrocortisone diffusion

Temporal variation

Figure 9 shows the temporal variation of the concentration of hydrocortisone in the receiver compartment of ICR (Fig. 9a) and SDR (Fig. 9b). In both cases, we can observe that the drug concentration increases with time. Figure 9a and b also illustrates the comparison of the diffusion of hydrocortisone for both young and old age. The general equation describing the variation in drug concentration reaching the receiver compartment is given in Eq. 13. The amount of drug left in the receiver compartment after sampling is given in Eq. 17.

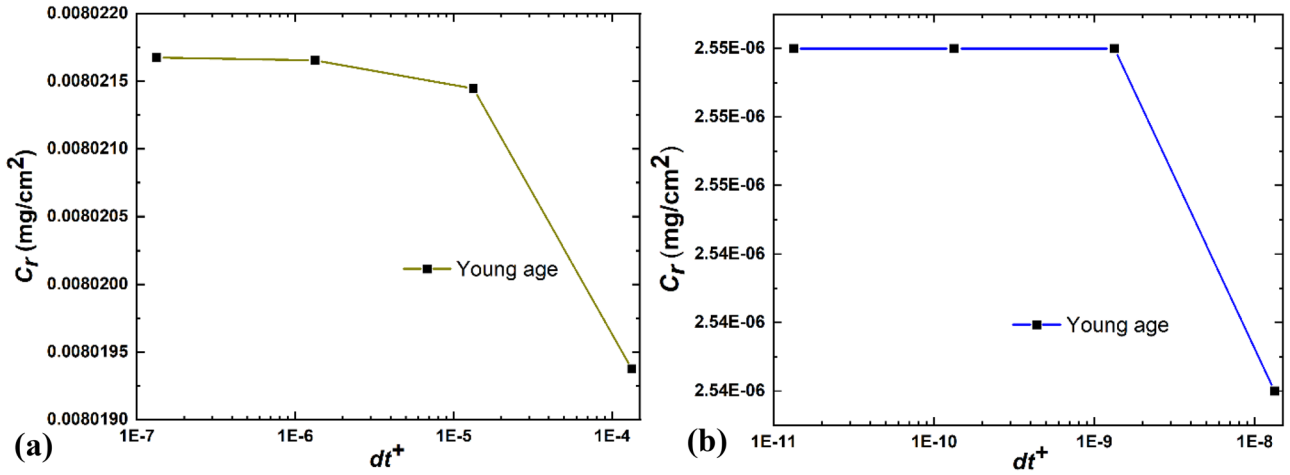

Fig. 8 Time independence for hydrocortisone diffusing through **a** intercellular route and **b** sweat duct route

Figure 9a shows the concentration (C_r) of hydrocortisone diffused in the receiver compartment though the ICR of old age is slightly more than that of young age. For example, after 20 min, the concentration (C_r) of hydrocortisone received in the receiver compartment is 0.079 mg/cm^2 for young age, whereas it is 0.085 mg/cm^2 for old age, which is 7.6% higher. This can be attributed to a slight decrease in the thickness of skin layers upon aging (Table 2). However, the concentration seems to be asymptotes with time; therefore, it reaches the same value in both young and old age after a long time.

The temporal variation of hydrocortisone in the receiver compartment diffusing through SDR for the two age groups has been illustrated in Fig. 9b. It can be inferred from the curve that there is a significant increase in the amount of drug diffusing through old age skin as compared to young age skin. After 60 min, we can see that 0.0134 µg/cm^2 and 0.0774 µg/cm^2 of the hydrocortisone had diffused through the SDR of young and old age, respectively. Compared to ICR, in the case of SDR, drug concentration (after 60 min) increases by 477% upon aging. Therefore, the effect of aging on drug delivery is found to be more significant in the sweat duct (SDR) than in the intercellular route (ICR). This can be attributed to an increase in pore size upon aging [43], which reduces the drag acting on drug particles and hence increases the diffusion coefficient or rate of diffusion. Also, upon aging, the length of the dermis decreases [42], which also contributes to an increase in the concentration gradient. However, in the case of the ICR, only skin layer thickness is the parameter that quantifies the aging effect on drug diffusion. As there is only a slight change in skin layer thickness, there is a minimal increment in the amount of drug permeated (through ICR) for aged people compared to young people.

One can find two significant differences when comparing Fig. 9a and b. It is found that the amount of drug diffusing through SDR is 1000 times less than that through ICR. This is due to the association of porosity and tortuosity with the SDR, which tends to reduce diffusion to a large extent. Due to pores, diffusing drugs will encounter drag force when passing through the SDR, and this, as well as the existence of tortuous pathways, reduces the concentration gradient. Physically, the existence of an outward flux inside the sweat duct and the presence of a tight junction may also lead to an additional barrier to drug diffusion. The second noticeable difference is that the time taken for hydrocortisone to reach a steady state is higher in the case of SDR than in ICR. This is due to the minimal rate of diffusion through SDR. Hence, a relatively large amount of time is required to reach a steady state.

Spatial variation through the intercellular route

Figure 10a and b represent the spatial variation of hydrocortisone diffusing through the ICR for young and old, respectively. Both figures show non-dimensional drug concentration variation (C^+) profile versus non-dimensional length (X^+) at $t = 0.05$, 5, and 60 min. Non-dimensional length, X^+ ranging from 0 to 1, shows the drug passing from the donor and reaching the first layer of ICR, the stratum corneum. However, the interface of the stratum corneum ($X^+ = 1$) provides a barrier to drug diffusion. This is considered by the partition coefficient, as shown in Eq. 22. The partition coefficient for the hydrocortisone permeating through the donor-sc interface is 8.22 (as shown in Table 1). This results

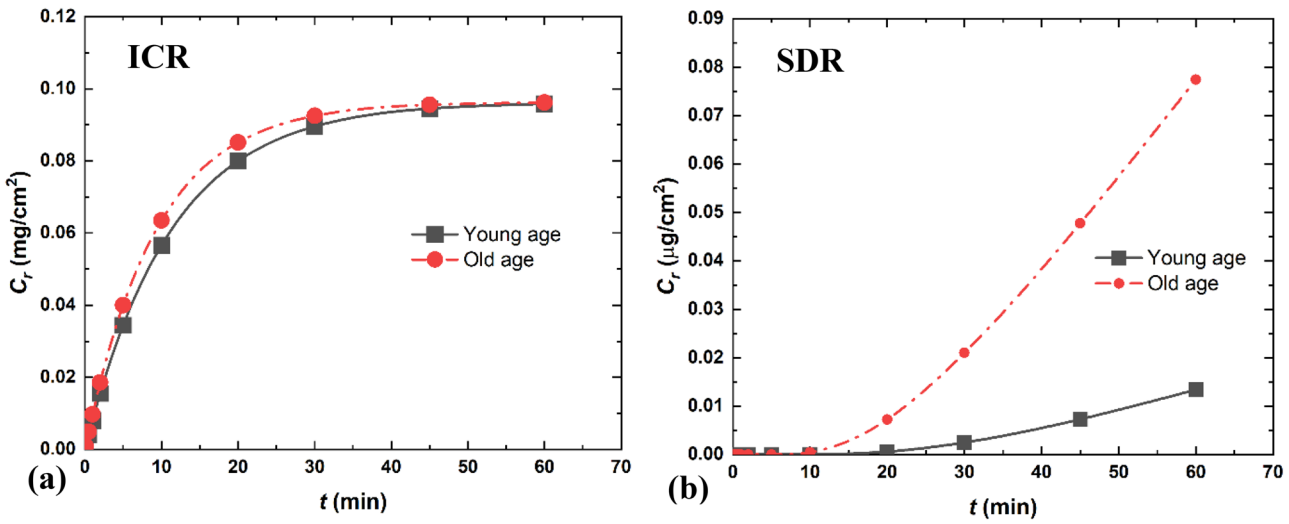

Fig. 9 Comparison of drug reaching the receiver compartment. Temporal variation of hydrocortisone (for young and old age) diffusing through **a** ICR and **b** SDR

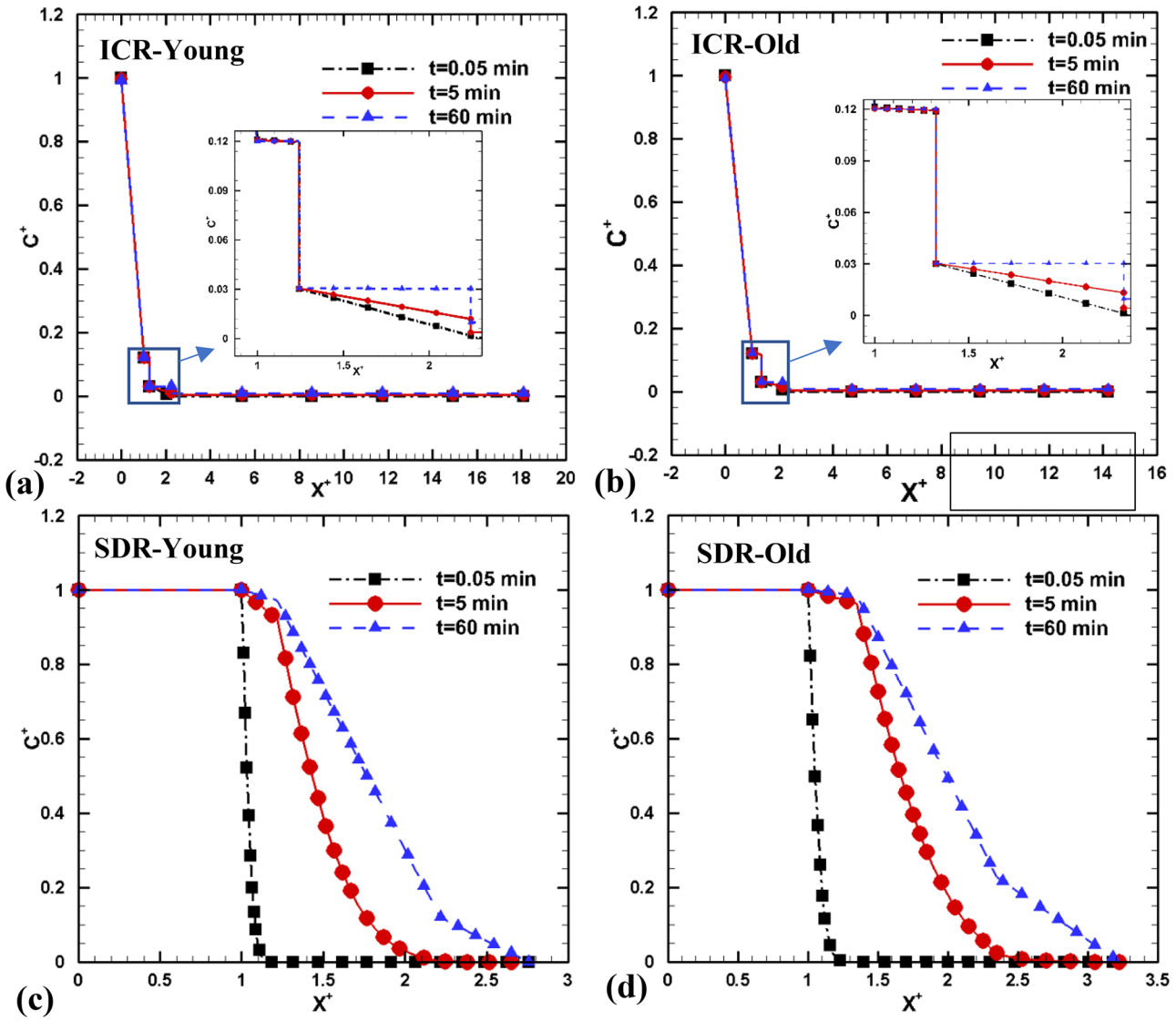

Fig. 10 Comparison of drug reaching the receiver compartment. Spatial variation of hydrocortisone diffusing through **a** ICR for young age, **b** ICR for old age, **c** SDR for young age, and **d** SDR for old age. Inset of **a** and **b** shows the jump in hydrocortisone concentration at the interface of ICR

in a drop in non-dimensional drug concentration (C^+), from 0.989 at $X^+ = 0$ (donor) to 0.119 at $X^+ = 1$ (sc) at the end of 60 min for young age. X^+ for stratum corneum ranges between 1 and 1.24 for the young age. The spatial variation of the drug in this region is given by Fick's law mentioned in Eq. 23. However, due to the small diffusion coefficient of hydrocortisone in the stratum corneum ($D_1 = 4.12 \times 10^{-5}$ cm^2/s), the rate of diffusion is found to be low.

Upon reaching the interface of the stratum corneum and viable epidermis, the drug encounters a new interface. Hence, it is accounted for by a different value of partition coefficient $K_2 = 3.94$ (Table 1). As per Eq. 24, at the interface, the amount of hydrocortisone partitioning and entering the viable epidermis is around 0.25 times less than the hydrocortisone in the stratum corneum. Equation 25 describes the drug concentration in the last grid point in the stratum corneum. At the stratum corneum and viable epidermis interface, a sharp drop in C^+ can be seen in the inset of Fig. 10a. C^+ drops from 0.119 to 0.03 at the interface between the stratum corneum and viable epidermis.

The spatial and temporal variation of hydrocortisone inside the viable epidermis is given in Eq. 26. Viable epidermis ranges between $X^+ = 1.24$ and 2.24 for the young age. The profile obtained in this region (at $t = 0.05$ min and 5 min) has a definite slope and becomes horizontal after achieving a steady state beyond $t = 45$ min. This is due to a lower value of drug diffusion coefficient in the viable epidermis ($D_2 = 9.61 \times 10^{-6}$ cm^2/s). Equation 27 considers the

partition coefficient ($K_3 = 3.11$) describing the drug concentration ratio in the viable epidermis to dermis at equilibrium. A drop-in concentration at this interface is observed in the inset of Fig. 10a. C^+ drops from 0.03 to 0.009 at this interface. The continuity of drug concentration between these two layers is ensured by interface conditions (Eq. 28).

Equation 29 describes hydrocortisone variation in the dermis layer as a function of space and time. The dermis layer ranges between $X^+ = 2.24$ and 18.08 at a young age. Among all three layers, hydrocortisone has the highest diffusion coefficient in the dermis layer ($D_3 = 8.45 \times 10^{-3}$ cm^2/s). This can be due to the coarser structure of the dermis layer, as discussed in the subsection of human skin anatomy. Therefore, due to the higher diffusion coefficient, the obtained concentration gradient is lower in the dermis layer (as seen in Fig. 10a).

Upon reaching the interface of the dermis and receiver, it is assumed that the receiver compartment imposes no restriction. This is why the partition coefficient is unity at this interface. Hence, the amount of hydrocortisone entering the receiver is the same as that leaving the dermis (Eq. 30). The temporal variation of hydrocortisone in the receiver compartment is given by Eq. 31. After 60 min, the non-dimensional hydrocortisone concentration (C^+) in the receiver compartment is found to be 0.009. Upon reaching the receiver compartment, it is assumed that 10.34% of the drug enters the blood capillaries (after each time step), from where it is carried away for systemic circulation. This has been mathematically accounted for by Eq. 17.

Figure 10b represents the spatial variation of non-dimensional hydrocortisone concentration (C^+) (diffusing through ICR) with non-dimensional length (X^+) for old age (> 60 years) at $t = 0.05$, 5, and 60 min. Upon aging, the stratum corneum's non-dimensional thickness (X^+) increases slightly from 0.24 to 0.33. A minimal increase in non-dimensional concentration gradient (from 0.00672 to 0.00674 after $t = 0.05$ min) is observed inside the stratum corneum. The non-dimensional thickness of the viable epidermis remains unchanged with age, and so is the concentration gradient. However, as the dermis layer thickness reduces significantly upon aging, this results in about a 2.24% increment in the concentration gradient. At the end of 0.05, 5, and 60 min, the amount of hydrocortisone reaching the receiver compartment increases by 51.51%, 16.34%, and 0.35%, respectively, for old age as compared to young age.

Spatial variation through the sweat duct route

Figure 10c represents the spatial variation of non-dimensional drug concentration in SDR (C^+) as a function of the non-dimensional thickness (X^+) for young age for $t = 0.05$, 5, and 60 min. Due to the tubular nature of this route, no interfaces are present, and hence there is no role of partition coefficient in drug diffusion. Therefore, no jump in C^+ is observed in Fig. 10c and d. However, pore size and tortuosity play a major role in drug permeation; hence, the diffusion coefficient for SDR is modified as per Eq. 33 [40].

$$D_e = D_w \zeta \varepsilon \tag{33}$$

where "ζ" is the apparent tortuosity (inverse of tortuosity) and "ε" represents the porosity. The diffusion coefficient of hydrocortisone in water is $D_w = 4.6 \times 10^{-6}$ cm^2/s (Table 1).

Similar to the ICR, Eqs. 38–50 are used to determine the hydrocortisone concentration in each layer of the sweat duct. The donor compartment lies in the range of $X^+ = 0$ to 1. Drug concentration in the donor compartment is constant with time as some amount of undissolved drug is always present in it. The upper coil duct ranges between $X^+ = 1$ and 1.22 for a young age. The porosity of this layer is 4.71×10^{-4} (as pore size of this layer is 20 µm) with a tortuosity of 1.22 for young age (Table 3). Since the rate of drug diffusion is low, therefore at $t = 0.05$ min, a small amount of drug is present in the upper coil duct of SDR. However, as time progresses (at $t = 5$ min and 60 min), a significant amount of drug diffuses through this layer. The dermal duct ranges between $X^+ = 1.22$ and 2.22. The pore size of this layer is 10 µm (porosity (ε) $= 1.17 \times 10^{-4}$) (less than that of the upper coil duct). However, tortuosity increases to 2 in this layer. Due to the reduction of pore size, the effective diffusion coefficient reduces, and hence diffusion rate also decreases. The secretory coil duct ranges between $X^+ = 2.22$ and $X^+ = 2.75$. The pore size in this layer increases to 30 µm, and tortuosity increases to 5.06.

Figure 10d represents the spatial variation of non-dimensional drug concentration (C^+) as a function of the non-dimensional thickness (X^+) for old age at $t = 0.05$, 5, and 60 min. The upper coil duct ranges between $X^+ = 1$ and 1.35 for old age. Table 3 shows that pore size increases upon aging. The porosity of the upper coiled duct increases from 4.71×10^{-4} to 4.24×10^{-3} upon aging. This increases the effective diffusion coefficient leading to faster diffusion. The dermal duct ranges between $X^+ = 1.35$ and 2.35 with a pore size of 20 µm and tortuosity of 2.72. In comparison, the secretory coil duct ranges between $X^+ = 2.35$ and 3.23 with a pore size of 40 µm and tortuosity of 3.82. As the pore size increases upon aging, the drag acting on a diffusing solution will also decrease. Because of this, the slope of the C^+ versus X^+ curve in Fig. 10d is more than that can be seen in Fig. 10c. Hence, as a result, the amount of drug diffusing through the sweat duct route increases upon aging.

At $t = 60$ min, the amount of hydrocortisone reaching the upper coil duct-dermal duct interface for old age is $C^+ = 0.984$ (compared to $C^+ = 0.971$ for young age). Similarly, the amount of hydrocortisone reaching the dermal duct-secretory coil duct

interface for old age is $C^+ = 0.227$ (compared to $C^+ = 0.119$ for young age). The amount of hydrocortisone entering the receiver compartment for old age is $C^+ = 0.00000786$ (compared to $C^+ = 0.00000136$ for young age) which is 477% higher. Therefore, it is found that drug diffusing through the SDR increases significantly upon aging.

Temporal and Spatial variation of benzoic acid diffusion

A similar kind of trend is observed in the case of benzoic acid for the spatial and temporal variation through the intercellular and sweat duct route (as shown in Figs. 11 and 12). However, one can observe that the amount of benzoic acid reaching the receiver compartment is more than the amount of hydrocortisone reaching the receiver compartment for both the intercellular and the sweat duct routes. This is arising due to the lower value of the drug partition coefficient and high value of the drug diffusion coefficient in stratum corneum compared to that of hydrocortisone (Table 1). However, the role of partition and diffusion coefficient of viable epidermis and dermis cannot be neglected. A lower partition coefficient value in the stratum corneum ensures that more amount of the drug is available for diffusion.

In contrast, a high diffusion coefficient value provides a high drug diffusion rate. Therefore, temporal variation of benzoic acid diffusing through the intercellular route, as shown in Fig. 11a, indicates that benzoic acid reaches a steady state (in around 1 min) faster than hydrocortisone (Fig. 9a) (after around 45 min) when diffusing through the intercellular route.

Figure 11a represents the temporal variation (C_r versus time (t)) of benzoic acid diffusing through the intercellular route. The amount of benzoic acid in the receiver compartment (left after sampling at the end of 1 min) when diffusing through the intercellular route is 0.854 mg/cm^2 for young age while 1.118 mg/cm^2 for old age. Hence, drug concentration increases by 2.84% upon aging when diffusing through ICR.

It is observed that the amount of benzoic acid diffusing through the sweat duct route (as shown in Fig. 11b) is more than that of hydrocortisone (Fig. 9b). This is because the diffusion coefficient of benzoic acid in water ($D_w = 1.16 \times 10^{-5}$ cm^2/s) is more than that of hydrocortisone in water ($D_w = 4.6 \times 10^{-6}$ cm^2/s) (Table 1). After 60 min, it is found that the amount of drug reaching the receiver compartment (after sampling) is 0.265 µg/cm^2 for old age while 0.057 µg/cm^2 for young age. Hence, the amount of benzoic acid increases by 364.9% upon aging.

Figure 12a and b represent the non-dimensional drug concentration (C^+) versus non-dimensional length (X^+) for young age and old age, respectively, for the ICR. As the diffusion coefficient of benzoic acid is higher than that of hydrocortisone (Table 1), it reaches a steady state much faster. Therefore, the spatial variation profile coincides at $t = 5$ and 60 min. Figure 12c and d represent the spatial variation of benzoic acid in SDR for young and old age, respectively. The trend is found to be similar to that in the case of diffusion of hydrocortisone through SDR (Fig. 10c and d).

Overall comparison

Apart from performing a numerical analysis of the permeation of hydrocortisone and benzoic acid through the intercellular and sweat duct route, an analysis of the

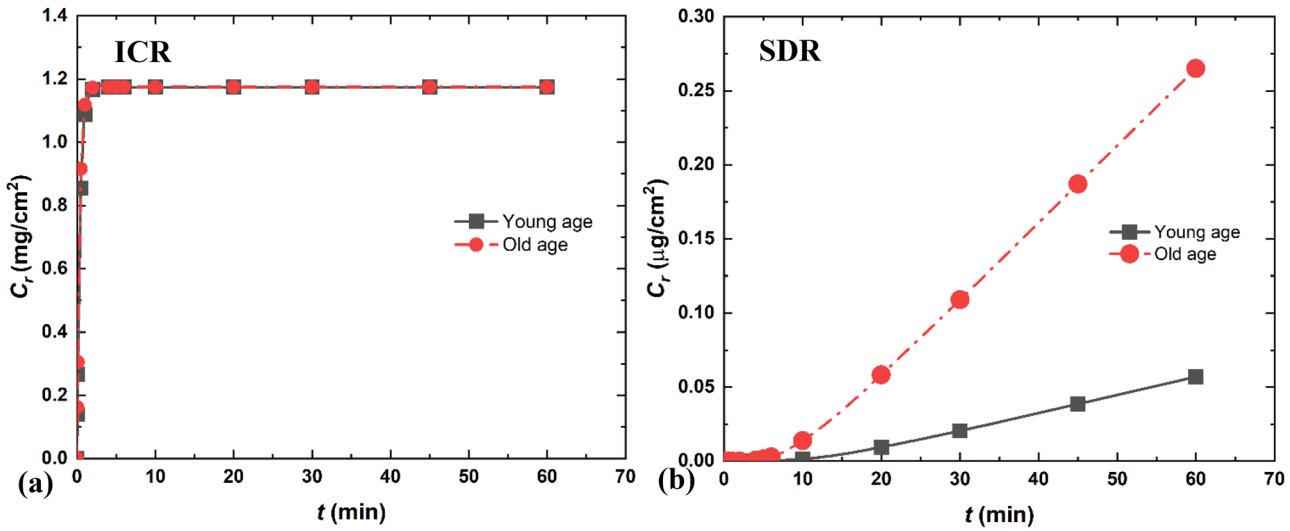

Fig. 11 Comparison of drug reaching the receiver compartment. Temporal variation of benzoic acid (for young and old age) diffusing through **a** ICR and **b** SDR

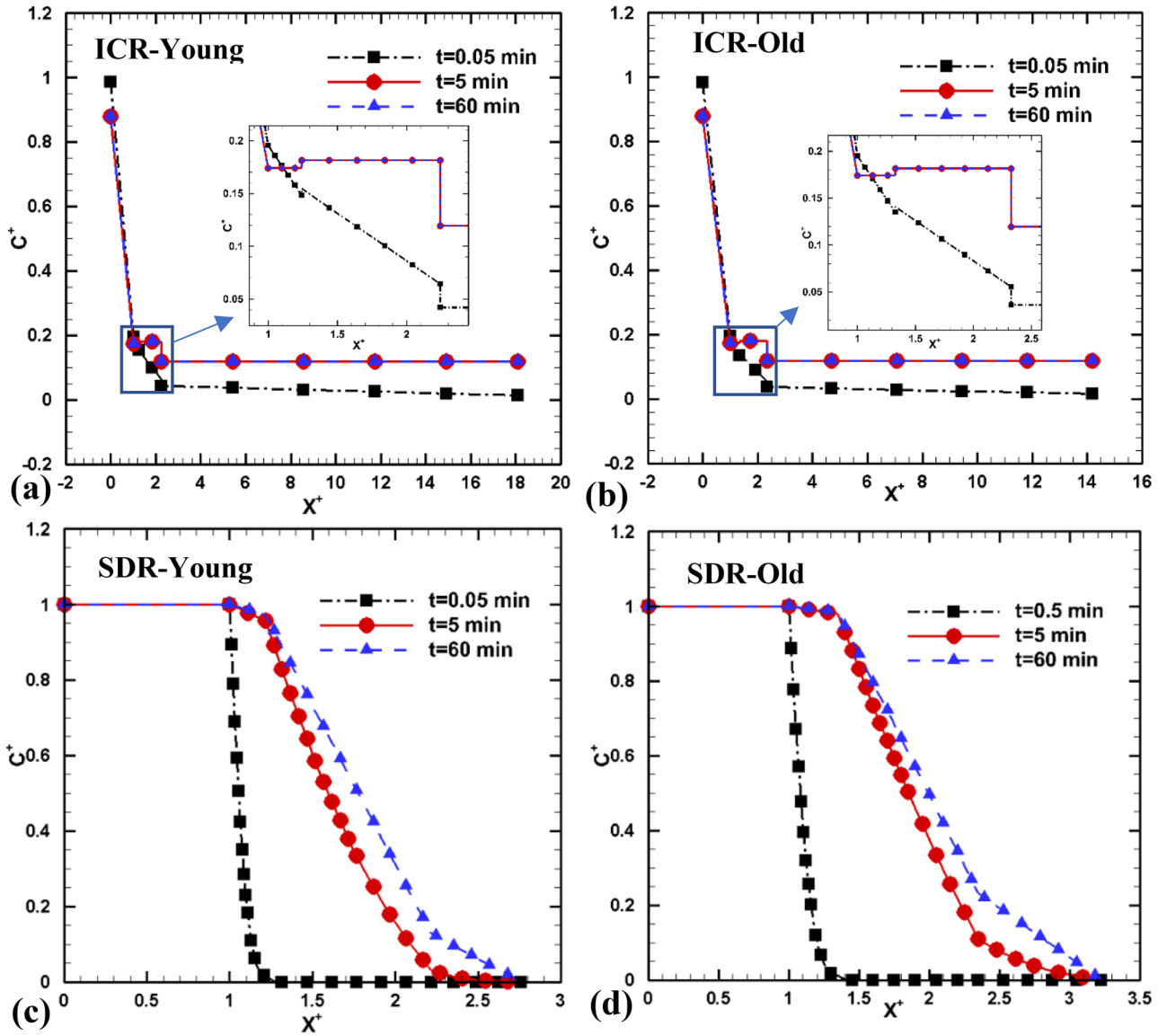

Fig. 12 Comparison of drug reaching the receiver compartment. Spatial variation of benzoic acid diffusing through **a** ICR for young age, **b** ICR for old age, **c** SDR for young age, and **d** SDR for old age. Inset of **a** and **b** shows the jump in benzoic acid concentration at the interface of ICR

diffusion of the solution of caffeine (Supplementary Figs. 1 and 2) and trans-cinnamic (Supplementary Figs. 3 and 4) is also performed. Similar trends are observed in these drugs' temporal and spatial variation profiles, as in the case of hydrocortisone and benzoic acid. For the sake of brevity, their results are not presented separately. However, to understand the overall comparison of all drugs, Fig. 13a and b illustrate the temporal variation of considered four drugs together through ICR and SDR, respectively. It also demonstrates the variation in the rate of permeation upon aging.

Intercellular route

Figure 13a represents the effect of aging on different drugs diffusing through the intercellular route. We can infer from this figure that drugs diffuse slightly faster in old than young age. Among all the considered drugs, benzoic acid (BA) is found to diffuse more through both ICR with a maximum value of 1.1741 mg/cm^2 for young and 1.1755 mg/cm^2 for old age (after 60 min). The least diffused drug is hydrocortisone (HC), with 0.0958 mg/cm^2 for young age and 0.0961 mg/cm^2 for old age (after 60 min). Drugs having

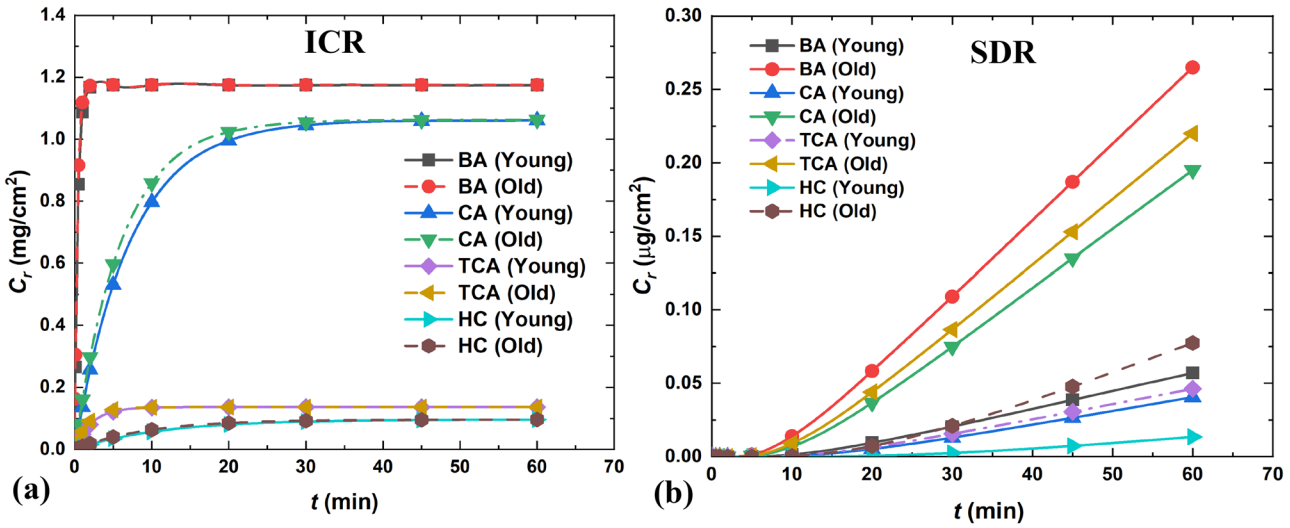

Fig. 13 Overall comparison of drugs diffusing through **a** intercellular route (ICR) and **b** sweat duct route (SDR) for young age (less than 40 years) and old age (greater than 60 years)

a relatively lower diffusion coefficient are found to diffuse relatively at a slower rate than benzoic acid and in a lesser amount due to a higher value of partition coefficient. After 60 min, the concentration of caffeine (CA) in the receiver compartment when diffusing through ICR is 1.061 mg/cm^2 for young and 1.062 mg/cm^2 for old age. While, for trans-cinnamic acid (TCA), after 60 min, it is found that 0.136 mg/cm^2 amount of the drug has diffused for young age and 0.1361 mg/cm^2 drug has diffused for old age.

Sweat duct route

Figure 13b represents the temporal variation of different drugs diffusing through the sweat duct route for young and old age. Like ICR, benzoic acid (BA) is found to diffuse in more amounts through SDR with a maximum value of 0.057 μg/cm^2 and 0.265 μg/cm^2 for young and old age respectively (after 60 min). The least diffused drug is hydrocortisone (HC), with 0.0134 μg/cm^2 for young age and 0.0774 μg/cm^2 for old age (after 60 min). In contrast, the amount of caffeine (CA) is found to be 0.0405 μg/cm^2 for young age and 0.195 μg/cm^2 for old age. The amount of trans-cinnamic acid (TCA) is found to be 0.0462 μg/cm^2 and 0.22 μg/cm^2 for young and old age, respectively, after 60 min.

Our study reveals the potential role of molecular weight and partition coefficient in permeation of drug through skin routes. Hence, there is scope for expanding the range of drugs that could be delivered as drug solutions through the skin. Further, our findings establish that drug permeation through the skin enhances upon aging. Hence, this can be exploited to deliver the drugs through transdermal mode to elderly people.

Conclusions

This work compares how drugs are delivered through the intercellular and sweat duct routes and finds that the intercellular route is more effective within the same time period. Among the drugs examined, benzoic acid has the highest rate of diffusion, while hydrocortisone has the lowest irrespective of the routes and age groups. The study shows that drug permeation increases with age, with drugs demonstrating significant increase in concentration when passing through both routes. This makes transdermal drug delivery a suitable option for continuous or low-dosage treatments for older individuals. The findings have the potential to contribute to the development of a real-time drug-tracking device that monitors how drugs permeate through the skin and circulate in the blood capillaries, enabling controlled drug delivery. However, before implementing such a device, the mathematical model needs refinement by considering biological factors such as permeability barriers, cell migration, tissue distribution, and the heterogeneous nature of human skin to ensure a more accurate representation of drug delivery mechanisms. Further, our current study represents a preliminary investigation focused on the effects of aging on drug diffusion through numerical analysis, and we fully recognize the significance of exploring functional excipients such as permeation enhancers in future research.

Appendix

This appendix section comprises equations related to sweat duct route (SDR). Set of Eqs. 1–11 has been converted into a non-dimensional form using Eq. 34. Similar to the intercellular route (ICR), Eqs. 35–38 describe the drug dissolution and variation of drug concentration in the donor compartment. Equations 39–49 represent the temporal and spatial variation of drug concentration within each layer of the sweat duct route (namely, upper coil duct (uc), dermal duct (dd), and secretory coil duct (sd)) (see Fig. 3b), as well as at the interface of each layer. Finally, using Eq. 50, the temporal variation of drug reaching the receiver compartment (viz., blood capillaries) is determined.

Characteristic variables to non-dimensionalize are:

$$C_d^+ = \frac{C_d}{C_{do}};\ C_r^+ = \frac{C_r}{C_{do}};\ t^+ = t\frac{D_{dd}^*}{h_{dd}^2};\ V_d^+ = \frac{V_d}{sh_{dd}};\ V_r^+ = \frac{V_r}{sh_{dd}};\ x^+ = 1 + \frac{x}{h_{dd}};\ K_t^+ = K_t\frac{h_{dd}^2}{D_{dd}^*} \tag{34}$$

Donor compartment

$$K_t^+ = \frac{4\Pi R_0^2 K_d h_{dd}^2}{V_d D_{dd}^*} \cdot R^{+2} \tag{35}$$

$$R^+ = \sqrt[3]{M^+} \tag{36}$$

$$M^+ = 1 + \left(\frac{C_{d0}Sh_{dd}}{M_0}\left(V_d^+\left(1 - C_d^+\right) - V_r^+ C_r^+ - \int_0^{h_{uc}} C_{uc}^+ dx^+ - \int_{h_{uc}}^{h_{uc}+h_{dd}} C_{dd}^+ dx^+ - \int_{h_{uc}+h_{dd}}^{h_{uc}+h_{dd}+h_{sd}} C_{sd}^+ dx^+\right)\right. \tag{37}$$

$$C_d^{+n+1} = C_d^{+n} + k_t^+ \Delta t^+ \left(C_s^+ - C_d^+\right) + \frac{D_{uc}^* \Delta t^+}{D_{dd}^* V_d^+} \cdot \frac{\left(C_{uc,i+1} - C_{uc.i}\right)}{\Delta x_{uc}^+} \tag{38}$$

Boundary of donor compartment and layer — upper coil duct

$$C_d^+|_{x^+=1} = k_1 C_{uc}^+ \tag{39}$$

Layer 1 (upper coil duct)

$$C_{uc,i}^{+n+1} = C_{uc,i}^{+n} + \frac{D_{uc}^* \Delta t^+}{D_{dd}^* \Delta x_{uc}^{+2}} \cdot \left(C_{uc,i-1}^{+n} - 2C_{uc,i}^{+n} + C_{uc,i+1}^{+n}\right) \tag{40}$$

Boundary of layer 1 — upper coil duct and layer 2 — dermal duct

$$C_{uc}^+|_{x^+=h_{uc}^+} = k_2 C_{dd}^+|_{x^+=h_{uc}^+} \tag{41}$$

$$C_{uc,i}^{+n} = \left(C_{uc,i+2}^{+n} + \frac{D_{uc}^* \Delta x_{dd}^+}{D_{dd}^* \Delta x_{uc}^+} \cdot C_{uc,i-1}^{+n}\right)/\left(1 + \frac{D_{uc}^* \Delta x_{dd}^+}{D_{dd}^* \Delta x_{uc}^+}\right) \tag{42}$$

Layer 2 — dermal duct

$$\frac{\partial C_{dd}^+}{\partial t^+} = \frac{D_{dd}^*}{D_{dd}^*} \cdot \frac{\partial^2 C_{dd}^+}{\partial x_{dd}^{+2}} \tag{43}$$

$$C_{dd,i}^{+n+1} = C_{dd,i}^{+n} + \frac{D_{dd}^* \Delta t^+}{D_{dd}^* \Delta x_{dd}^{+2}} \cdot \left(C_{dd,i-1}^{+n} - 2C_{dd,i}^{+n} + C_{dd,i+1}^{+n}\right) \tag{44}$$

Boundary of layer 2 — dermal duct and layer 3 — secretory coil duct

$$C_{dd}^+|_{x^+=h_{dd}^+} = k_3 C_{sd}^+|_{x^+=h_{dd}^+} \tag{45}$$

$$C_{dd,i}^{+n} = \left(C_{dd,i-1}^{+n} + \frac{D_{sd}^* \Delta x_{dd}^+}{D_{dd}^* \Delta x_{sd}^+} \cdot C_{sd,i+2}^{+n}\right)/\left(1 + k_3 * \frac{D_{sd}^* \Delta x_{dd}^+}{D_{dd}^* \Delta x_{sd}^+}\right) \tag{46}$$

Layer 3 — secretory coil duct

$$\frac{\partial C_{sd}^+}{\partial t^+} = \frac{D_{sd}^*}{D_{dd}^*} \cdot \frac{\partial^2 C_{sd}^+}{\partial x_{sd}^{+2}} \tag{47}$$

$$C_{sd,i}^{+n+1} = C_{sd,i}^{+n} + \frac{D_{sd}^* \Delta t^+}{D_{dd}^* \Delta x_{sd}^{+2}} \cdot \left(C_{sd,i-1}^{+n} - 2C_{sd,i}^{+n} + C_{sd,i+1}^{+n}\right) \tag{48}$$

Boundary of layer 3 — secretory coil duct and receiver compartment

$$C_{r,i}^{+n} = C_{sd,i-1}^{+n} \tag{49}$$

Receiver compartment

$$C_{r,i}^{+n+1} = C_{r,i}^{+n} + \frac{D_{sd}^* \Delta t^+}{V_r^+ D_{dd}^*} \cdot \frac{\left(C_{sd,i-2}^{+n} - C_{sd,i-1}^{+n}\right)}{\Delta x_{sd}^+} \tag{50}$$

Supplementary Information The online version contains supplementary material available at https://doi.org/10.1007/s13346-024-01529-6.

Acknowledgements N.D.P. gratefully acknowledges the financial support under the startup-research-grant (SRG) scheme from the Science and Engineering Research Board (SERB), Department of Science and Technology, Government of India, New Delhi, by Grant No. SRG/2020/001947, for the computational workstation used in the present work's simulation.

Author contribution All authors contributed to the study conception and design. Methodology and code development, drug selection for testing, data collection, and analysis were performed by first author Aditya Ranjan. The first draft of the manuscript was written by Aditya

Ranjan. Vijay S. Duryodhan and Nagesh D. Patil supervised this work and reviewed and edited the manuscript. All authors read and approved the final manuscript.

Availability of data and materials The datasets generated during and/or analyzed during the current study are available from the corresponding author on reasonable request.

Declarations

Ethics approval and consent to participate Not applicable.

Consent for publication All the authors gave their consent for publication of this manuscript in this journal and the work has not been published and is not being considered for publication elsewhere. In this work, informed consent is not applicable as this work is a computational study.

Competing interests The authors declare no competing interests.

References

1. Brown MB, Martin GP, Jones SA, Akomeah FK. Dermal and transdermal drug delivery systems: current and future prospects. Drug Deliv. 2006;13(3):175–87. https://doi.org/10.1080/10717540500455975.
2. Duvvuri S, Majumdar S, Mitra AK. Role of metabolism in ocular drug delivery. Curr Drug Metab. 2004;5(6):507–15. https://doi.org/10.2174/1389200043335342.
3. Newman SP. Drug delivery to the lungs: challenges and opportunities. Ther Deliv. 2017;8(8):647–61. https://doi.org/10.4155/tde-2017-0037.
4. Bischoff JE, Arruda EM, Grosh K. Finite element modeling of human skin using an isotropic, nonlinear elastic constitutive model. J Biomech. 2000;33(6):645–52. https://doi.org/10.1016/s0021-9290(00)00018-x.
5. Trommer H, Neubert RHH. Overcoming the stratum corneum: the modulation of skin penetration. A review Skin Pharmacol Physiol. 2006;19(2):106–21. https://doi.org/10.1159/000091978.
6. Hussain JN, Mantri N, Cohen MM, Hussain J. Working up a good sweat-the challenges of standardising sweat collection for metabolomics analysis. Clin Biochem Rev. 2017;38(1):13–34.
7. Otberg N, Richter H, Schaefer H, Blume-Peytavi U, Sterry W, Lademann J. Variations of hair follicle size and distribution in different body sites. J Invest Dermatol. 2004;122(1):14–9. https://doi.org/10.1046/j.0022-202x.2003.22110.x.
8. Tojo K. Random brick model for drug transport across stratum corneum. J Pharm Sci. 1987;76(12):889–91. https://doi.org/10.1002/jps.2600761209.
9. Prausnitz MR, Langer R. Transdermal drug delivery. Nat Biotechnol. 2008;26(11):1261–8. https://doi.org/10.1038/nbt.1504.
10. Andrews SN, Jeong E, Prausnitz MR. Transdermal delivery of molecules is limited by full epidermis, not just stratum corneum. Pharm Res. 2013;30(4):1099–109. https://doi.org/10.1007/s11095-012-0946-7.
11. Meidan VM, Bonner MC, Michniak BB. Transfollicular drug delivery - is it a reality? Int J Pharm. 2005;306:1–14.
12. Bovell D. The human eccrine sweat gland: structure, function and disorders. J Local Global Health Sci. 2015;2015(1):5. https://doi.org/10.5339/jlghs.2015.5.
13. Rabost-Garcia G, Farré-Lladós J, Casals-Terré J. Recent impact of microfluidics on skin models for perspiration simulation. Membranes (Basel). 2021;11(2):150. https://doi.org/10.3390/membranes11020150.
14. Wilke K, Wepf R, Keil FJ, Wittern KP, Wenck H, Biel SS. Are sweat glands an alternate penetration pathway? Understanding the morphological complexity of the axillary sweat gland apparatus. Skin Pharmacol Physiol. 2006;19(1):38–49. https://doi.org/10.1159/000089142.
15. Shim J, Seok Kang H, Park WS, Han SH, Kim J, Chang IS. Transdermal delivery of mixnoxidil with block copolymer nanoparticles. J Control Release. 2004;97(3):477–84. https://doi.org/10.1016/j.jconrel.2004.03.028.
16. Meidan VM, Docker M, Walmsley AD, Irwin WJ. Pharm Res. 1998;15(1):85–92. https://doi.org/10.1023/a:1011956905388.
17. Walicka A, Iwanowska-Chomiak B. Drug diffusion transport through human skin. Int J Appl Mech Eng. 2018;23(4):977–88. https://doi.org/10.2478/ijame-2018-0055.
18. Coceani N, Colombo I, Grassi M. Acyclovir permeation through rat skin: mathematical modelling and in vitro experiments. Int J Pharm. 2003;254(2):197–210. https://doi.org/10.1016/s0378-5173(03)00028-0.
19. Pineau A, Guillard O, Favreau F, Marrauld A, Fauconneau B. In vitro study of percutaneous absorption of aluminum from antiperspirants through human skin in the Franz™ diffusion cell. J Inorg Biochem. 2012;110:21–6. https://doi.org/10.1016/j.jinorgbio.2012.02.013.
20. Neupane R, Boddu SHS, Renukuntla J, Babu RJ, Tiwari AK. Alternatives to biological skin in permeation studies: current trends and possibilities. Pharmaceutics. 2020;12(2):152. https://doi.org/10.3390/pharmaceutics12020152.
21. Bartosova L, Bajgar J. Transdermal drug delivery in vitro using diffusion cells. Curr Med Chem. 2012;19(27):4671–7. https://doi.org/10.2174/092986712803306358.
22. George K, Kubota K, Twizell EH. A two-dimensional mathematical model of percutaneous drug absorption. Biomed Eng Online. 2004;3(1):18. https://doi.org/10.1186/1475-925x-3-18.
23. Grassi M, Colombo I. Mathematical modelling of drug permeation through a swollen membrane. J Control Release. 1999;59(3):343–59. https://doi.org/10.1016/s0168-3659(98)00198-9.
24. Sugibayashi K, Todo H, Oshizaka T, Owada Y. Mathematical model to predict skin concentration of drugs: toward utilization of silicone membrane to predict skin concentration of drugs as an animal testing alternative. Pharm Res. 2010;27(1):134–42. https://doi.org/10.1007/s11095-009-9987-y.
25. Cygan RT, Ho CK, Weiss CJ. Linking the geosciences to emerging bio-engineering technologies. 2002.
26. Shen L, Chen Z. Critical review of the impact of tortuosity on diffusion. Chem Eng Sci. 2007;62(14):3748–55. https://doi.org/10.1016/j.ces.2007.03.041.
27. Chaulagain B, Jain A, Tiwari A, Verma A, Jain SK. Passive delivery of protein drugs through transdermal route. Artif Cells Nanomed Biotechnol. 2018;46(sup1):472–87. https://doi.org/10.1080/21691401.2018.1430695.
28. Ellison CA, Tankersley KO, Obringer CM, Carr GJ, Manwaring J, Rothe H, Duplan H, Géniès C, Grégoire S, Hewitt NJ, Jamin CJ, Klaric M, Lange D, Rolaki A, Schepky A. Partition coefficient and diffusion coefficient determinations of 50 compounds in human intact skin, isolated skin layers and isolated stratum corneum lipids. Toxicol In Vitro. 2020;69(104990): 104990. https://doi.org/10.1016/j.tiv.2020.104990.
29. Delgado JMPQ. Molecular diffusion coefficients of organic compounds in water at different temperatures. J Phase Equilibria Diffus. 2007;28(5):427–32. https://doi.org/10.1007/s11669-007-9160-4.
30. di Cagno MP, Clarelli F, Våbenø J, Lesley C, Rahman SD, Cauzzo J, Franceschinis E, Realdon N, Stein PC. Experimental

determination of drug diffusion coefficients in unstirred aqueous environments by temporally resolved concentration measurements. Mol Pharm. 2018;15(4):1488–94. https://doi.org/10.1021/acs.molpharmaceut.7b01053.
31. Shahi V, Zatz JL. Effect of formulation factors on penetration of hydrocortisone through mouse skin. J Pharm Sci. 1978;67(6):789–92. https://doi.org/10.1002/jps.2600670615.
32. Tripathi SR, Miyata E, Ishai PB, Kawase K. Morphology of human sweat ducts observed by optical coherence tomography and their frequency of resonance in the terahertz frequency region. Sci Rep. 2015;5(1):9071. https://doi.org/10.1038/srep09071.
33. Koeke PU, Parizotto NA, Carrinho PM, Salate ACB. Comparative study of the efficacy of the topical application of hydrocortisone, therapeutic ultrasound and phonophoresis on the tissue repair process in rat tendons. Ultrasound Med Biol. 2005;31(3):345–50. https://doi.org/10.1016/j.ultrasmedbio.2004.12.005.
34. Holmgaard R, Benfeldt E, Nielsen JB, Gatschelhofer C, Sorensen JA, Höfferer C, Bodenlenz M, Pieber TR, Sinner F. Comparison of open-flow microperfusion and microdialysis methodologies when sampling topically applied fentanyl and benzoic acid in human dermis ex vivo. Pharm Res. 2012;29(7):1808–20. https://doi.org/10.1007/s11095-012-0705-9.
35. Luo L, Lane ME. Topical and transdermal delivery of caffeine. Int J Pharm. 2015;490(1–2):155–64. https://doi.org/10.1016/j.ijpharm.2015.05.050.
36. Smith CK, Moore CA, Elahi EN, Smart AT, Hotchkiss SA. Human skin absorption and metabolism of the contact allergens, cinnamic aldehyde, and cinnamic alcohol. Toxicol Appl Pharmacol. 2000;168(3):189–99. https://doi.org/10.1006/taap.2000.9025.
37. Ellis RA, Montagna W, Fanger H. Histology and cytochemistry of human skin. XIV. The blood supply of the cutaneous glands**from the department of biology, brown university and department of pathology, Rhode Island hospital, providence, Rhode Island. J Invest Dermatol. 1958;30(3):137–45. https://doi.org/10.1038/jid.1958.26.
38. Kurosumi K, Shibasaki S, Ito T. Cytology of the secretion in mammalian sweat glands. Int Rev Cytol. 1984;87:253–329. https://doi.org/10.1016/s0074-7696(08)62445-6.
39. Saxena SK, Boersma L, Lindstrom FT, Young JL. Effect of pore size on diffusion coefficients in porous media. Soil Sci. 1974;117(2):80–6. https://doi.org/10.1097/00010694-197402000-00002.
40. Shackelford CD, Moore SM. Fickian diffusion of radionuclides for engineered containment barriers: diffusion coefficients, porosities, and complicating issues. Eng Geol. 2013;152(1):133–47. https://doi.org/10.1016/j.enggeo.2012.10.014.
41. Waller JM, Maibach HI. Age and skin structure and function, a quantitative approach (I): blood flow, pH, thickness, and ultrasound echogenicity. Skin Res Technol. 2005;11(4):221–35. https://doi.org/10.1111/j.0909-725X.2005.00151.x.
42. Ezure T, Amano S, Matsuzaki K. Aging-related shift of eccrine sweat glands toward the skin surface due to tangling and rotation of the secretory ducts revealed by digital 3D skin reconstruction. Skin Res Technol. 2021;27(4):569–75. https://doi.org/10.1111/srt.12985.
43. Flament F, Francois G, Qiu H, Ye C, Hanaya T, Batisse D, Cointereau-Chardon S, Seixas MDG, Dal Belo SE, Bazin R. Facial skin pores: a multiethnic study. Clin Cosmet Investig Dermatol. 2015;8:85–93. https://doi.org/10.2147/CCID.S74401.